

A SAMPLE OF CANDIDATE RADIO STARS IN FIRST AND SDSS

AMY E. KIMBALL¹, GILLIAN R. KNAPP², ŽELJKO IVEZIĆ¹, ANDREW A. WEST³, JOHN J. BOCHANSKI³, RICHARD M. PLOTKIN¹,
AND MICHAEL S. GORDON²

¹ Department of Astronomy, University of Washington, Box 351580, Seattle, WA 98195-1580, USA; akimball@astro.washington.edu

² Department of Astrophysical Sciences, Princeton University, Princeton, NJ 08544, USA

³ Kavli Institute for Astrophysics and Space Research, Massachusetts Institute of Technology, Cambridge, MA 02139, USA

Received 2009 January 14; accepted 2009 June 12; published 2009 July 24

ABSTRACT

We conduct a search for radio stars by combining radio and optical data from the FIRST survey and the Sloan Digital Sky Survey (SDSS). The faint limit of SDSS makes possible a homogeneous search for radio emission from stars of low optical luminosity. We select a sample of 112 candidate radio stars in the magnitude range $15 < i \lesssim 19.1$ and with radio flux $S_{20} \geq 1.25$ mJy, from about 7000 deg² of sky. The selection criteria are positional coincidence within 1", radio and optical point source morphology, and an SDSS spectrum classified as stellar. The sample contamination is estimated by random matching to be 108 ± 13 , suggesting that at most a small fraction of the selected candidates are genuine radio stars. Therefore, we rule out a very rare population of extremely radio-loud stars: no more than 1.2 of every million stars in the magnitude range $15 < i < 19.1$ stars has radio flux $S_{20} \geq 1.25$ mJy. We investigate the optical and radio colors of the sample to find candidates that show the largest likelihood of being real radio stars. The significant outliers from the stellar locus, as well as the magnetically active stars, are the best candidates for follow-up radio observations. We conclude that, while the present wide-area radio surveys are not sensitive enough to provide homogeneous samples of the extremely rare radio stars, upcoming surveys that exploit the great sensitivity of current and planned telescopes do have sufficient sensitivity and will allow the properties of this class of object to be investigated in detail.

Key words: radio continuum: stars – stars: statistics – surveys

Online-only material: color figures and machine-readable tables

1. INTRODUCTION

The light from stars dominates the optical sky, while the radio sky's contribution from stars is very small. However, significant radio emission has been detected from *active* stars in the form of synchrotron, gyrosynchrotron, or electron cyclotron maser emission (Dulk 1985; Güdel 2002). Some of the nonthermal processes that lead to these types of emission—plasma heating and particle acceleration in stellar coronae—are seen in our own Sun, but the relevant energies for active stars are much larger. Radio emission at the relative level of that emitted by the Sun remains undetected from even the closest solar-type main-sequence stars to the present day.⁴ The quiescent, slowly varying radio emission seen in many active stars (e.g., Güdel 2002, and references therein) has no solar counterpart.

With the great increase in the sensitivity of radio surveys in the last several decades, along with the more accurate source positions allowed by radio interferometry, both thermal and nonthermal radio emission have now been detected from hundreds of stars of many different types (Hjellming & Gibson 1986; Wendker 1987; Altenhoff et al. 1994; Wendker 1995). These include pre-main-sequence stars (T Tau and Herbig Ae/Be⁵ stars; Güdel et al. 1989; White et al. 1992; Skinner et al. 1993), rapidly rotating main-sequence stars (Lim & White 1995; Berger 2002), X-ray bright main-sequence stars (Güdel et al. 1995), magnetic stars (Drake et al. 1987a; Leone et al. 1996; Berger 2006; Berger et al. 2008), cool giants with extended chromospheres and photospheres (Newell & Hjellming 1982; Drake & Linsky 1986; Drake et al. 1987b;

Knapp et al. 1995; Reid & Menten 1997), OB stars with winds (Bieging et al. 1989; Drake 1990; Phillips & Titus 1990), Wolf-Rayet stars (Chapman et al. 1999), dMe flare stars (White et al. 1989; Osten et al. 2006), and various classes of interacting binaries and cataclysmic variables. The radio radiation from these stars is very faint, at the few mJy level.

The first large unbiased study of radio stars (~ 5000 deg² of sky at high galactic latitude) was performed by Helfand et al. (1999, hereafter H99), who compared the Faint Images of the Radio Sky at Twenty cm survey (FIRST; Becker et al. 1995) to several catalogs of bright stars with high astrometric precision: the Hipparcos catalog (Perryman et al. 1997), the Tycho catalog (Hoeg et al. 1997), the Guide Star Catalog (Lasker et al. 1990), and stars within 25 pc of the Sun. They emphasized the need for accurate positions: the rarity of radio stars to the FIRST flux limit (~ 1 mJy), combined with the high density of faint extragalactic radio sources, ensures random matches between stellar and radio sources in sufficient numbers to confuse the cataloging of true radio stars, unless both radio and optical positions are known to better than 1". H99 identified 26 radio stars in their study, about one per 190 deg², and showed that the fraction of stars with radio emission above the FIRST limit declines steeply with optical magnitude to $m_V \gtrsim 15$. The fraction of radio stars at fainter magnitudes is unknown. Kimball & Ivezić (2008, hereafter KI08) searched for radio stars in a combined radio–optical catalog with observations from FIRST and from the optical Sloan Digital Sky Survey (SDSS). Quasars are the most common radio source above flux densities of a few mJy; therefore, a sample of optical point sources with radio emission is likely to be strongly dominated by quasars. KI08 approached this problem by applying a conservative photometric color cut, using the fact that quasars and stars lie in different locations in SDSS optical color–color diagrams (Richards et al. 2001). The

⁴ Typical radio flux from a star identical to the Sun, and with apparent magnitude $m_V = 20$, would reach about 3.0×10^{-6} mJy.

⁵ The “e” following the spectral class indicates emission in the spectrum.

sample was limited to sources sufficiently bright to be included in the SDSS quasar spectroscopic target selection ($i < 19.1$; Schneider et al. 2007). Only 20% of the photometrically selected candidate radio stars actually showed stellar spectra, while the rest were quasars with stellar-like colors. KI08 concluded that simple color criteria are not sufficient to select a clean sample of radio stars and that spectroscopic observations are necessary to distinguish between quasars and stars.

In this paper, we continue the search for radio stars in the SDSS using a sample with spectroscopic identifications. We present 112 candidates selected by matching FIRST detections and SDSS point sources within 1 arcsec. The sample comprises sources brighter than $r = 20.5$ in the optical and 1.25 mJy at 20 cm, with SDSS spectra classified as stellar both by the automated reduction pipelines and visually. The SDSS spectroscopic targeting implicitly imposes soft magnitude limits of $15 < i \lesssim 19.1$. In this magnitude range, approximately 1% of SDSS stars have spectroscopic data. However, *all* objects in this range that are close to a FIRST source are targeted for spectra (Stoughton et al. 2002), so the completeness of SDSS radio–optical sources is well understood.

We are searching in a different region of the radio–optical parameter space from H99, who also matched to FIRST but used optical catalogs brighter than $m_v = 15$. The SDSS has a saturation limit of $m_i = 15$. By extending to several optical magnitudes fainter than H99, we therefore search for stars with a much brighter radio-to-optical flux ratio. However, a FIRST–SDSS matching has the potential to reveal a radio-bright population too rare to appear in the smaller H99 study, as the fainter SDSS includes a much larger volume in the Galaxy. For example, M dwarfs, many of which are known to be magnetically active (e.g., West et al. 2008), are found in significant numbers only at faint magnitudes. Thus, a search for radio-emitting M dwarfs should be carried out in a deep optical survey with large sky coverage. Advantages to using the SDSS are its high completeness, precise magnitudes, accurate astrometry, much deeper optical data than previous stellar catalogs, and almost 300,000 stellar spectra.

The remainder of the paper is laid out as follows. In Section 2, we describe the contributing surveys. In Section 3, we outline the selection of the sample of radio stars and place an upper limit on the fraction of radio stars. In Sections 4 and 5, we discuss optical and radio properties of the sample, respectively, and in Section 6 we conclude and summarize our results.

2. OPTICAL AND RADIO DATA

2.1. Optical Catalog: SDSS

We have drawn our sample from the photometric coverage of the sixth data release (DR6) of the SDSS⁶ (see York et al. 2000; Stoughton et al. 2002; Adelman-McCarthy et al. 2008, and references therein). DR6 covers roughly 9600 deg^2 and contains photometric observations for 287 million unique objects, as well as spectra for more than 1 million sources (in a smaller sky area of 6860 deg^2). SDSS entered routine operations in 2000; DR6 observations were completed in 2006 June. Because SDSS spectroscopy is performed after photometric observations, some stars in the sample have spectra that were not available until the seventh data release (DR7). We have included some stars with DR7 spectra⁷; we point out explicitly where this detail

⁶ The survey Web site is located at <http://www.sdss.org>.

⁷ We include stars with spectroscopic observations taken through 2007 December 5.

affects our estimates of sample contamination in Section 3.6. The DR6 sample includes about 287,000 spectra classified as stars.

The SDSS photometric survey measures flux densities nearly simultaneously in five wavelength bands ($u, g, r, i,$ and z) with effective wavelengths of 3551, 4686, 6165, 7481, and 8931 Å (Fukugita et al. 1996; Gunn et al. 1998; Hogg et al. 2001; Tucker et al. 2006; Smith et al. 2002; Ivezić et al. 2004). Morphology information allows reliable star–galaxy separation to $r \sim 21.5$ (Lupton et al. 2002; Scranton et al. 2002). Sources are classified as resolved or unresolved using a measure of light concentration that determines how well the flux resembles a point source (Stoughton et al. 2002). Magnitudes were corrected for Galactic extinction according to the dust maps of Schlegel et al. (1998). The astrometry of the photometric survey is good to $\lesssim 0.1$ (Pier et al. 2003).

A subset of photometric sources was chosen for spectroscopy according to the SDSS targeting pipeline; stars could be serendipitously selected by any of the various targeting algorithms. The quasar targeting algorithm selects all $15 < i < 19.1$ sources within $2''$ of a FIRST catalog object, and some sources as faint as $i = 20.5$ (depending on the availability of spectral fibers). About 30% of quasar targets turn out to be stars or galaxies (Schneider et al. 2007). Another algorithm targets interesting stellar classes by selecting for their distinctive photometric colors; these include blue horizontal-branch stars, carbon stars, subdwarfs, cataclysmic variables, brown and red dwarfs, and white dwarfs. Because stars in these categories are selected randomly to fill excess spectral fibers, the completeness of the samples of stars with spectroscopic observations is, with a small number of exceptions, not well defined. However, the fact that all objects within $2''$ of a FIRST source are targeted implies that the spectroscopic sample is complete to $i < 19.1$ with respect to radio–optical sources brighter than the FIRST limit, except in the case of fiber collisions (see below).

SDSS spectra are obtained using $3''$ fibers in a fiber-fed spectrograph (Newman et al. 2004). Spectra cover the wavelength range from about 3500 to 9500 Å with a resolution of $R \sim 1800$. They are automatically extracted and calibrated by the Spectroscopic Pipeline: wavelength calibrations are calculated from arc and night sky lines and flux calibrations from observations of standard F stars. Some fibers are used to observe blank sky in order to correct targeted objects for the sky spectrum. Not every object targeted for spectroscopy obtains a spectrum, primarily because of fiber collisions: due to the physical size of the fibers, no two fibers can be placed closer than $55''$ on a spectroscopic plate. As a result, spectra are only taken for about 92.5% of spectroscopic targets, although the completeness effects are well understood (Blanton et al. 2003).

2.2. Radio Catalogs

FIRST provides 20 cm radio fluxes, which were used to select candidate radio stars. The Westerbork Northern Sky Survey (WENSS) and the Green Bank 6 cm (GB6) survey provide fluxes at 92 cm and 6 cm, respectively, which allow us to determine a radio spectral shape.

2.2.1. FIRST

The FIRST survey (Becker et al. 1995) used the Very Large Array to observe the sky at 20 cm (1.4 GHz) with a beam size of $5.4''$ and an rms sensitivity of about $0.15 \text{ mJy beam}^{-1}$. Designed to cover the same region of sky as the SDSS, FIRST observed 9000 deg^2 at the North Galactic Cap and a smaller

~ 2.5 wide strip along the Celestial Equator from 1994 to 2002. The survey contains over 800,000 unique sources, with positions determined to $\lesssim 1''$; its source density is roughly 97 deg^{-2} . It is 95% complete to 2 mJy and 80% complete to the survey limit of 1 mJy. The integrated flux density, S_{20} , is calculated using a two-dimensional Gaussian fit to each source image.

2.2.2. WENSS

WENSS (Rengelink et al. 1997) is a 92 cm radio survey that was conducted in the mid-1990s. It observed the sky north of $\delta = 29^\circ$ to a limiting flux density of 18 mJy, with a beam size of $54''$ and a positional uncertainty of $1''.5\text{--}5''$.

2.2.3. GB6

The GB6 survey at 4.85 GHz (Gregory et al. 1996) was executed with the original 91 m Green Bank telescope in 1986 November and 1987 October. Data from both epochs were assembled into a survey covering the $0^\circ < \delta < 75^\circ$ sky down to a limiting flux of 18 mJy, with 3.5 resolution and a positional uncertainty of $10''\text{--}50''$.

3. SELECTING A SAMPLE OF CANDIDATE RADIO STARS FROM FIRST AND SDSS

This section outlines the selection criteria that yield the candidate radio stars sample. We estimate the amount of contamination with random matching and use the result to place an upper limit on the fraction of radio stars in the magnitude range of the sample. The area of overlap of the two surveys is about 9500 deg^2 .

3.1. Magnitude and Flux Limits

We applied magnitude/flux limits as a way to control source quality. For SDSS sources, we required $r < 20.5$ to ensure reliable determination of optical morphology as well as to select sources with a high enough signal-to-noise ratio (S/N) for spectral typing. Owing to the magnitude limits of the SDSS quasar target selection algorithm (Section 2.1), most of the sources in the final sample have $i \lesssim 19.1$, although it is not an explicit requirement. There are roughly 4000–5000 SDSS sources with $r < 20.5$ per square degree on the sky, depending on Galactic latitude.

For the radio sources, we adopted a limit of $S_{20} \geq 1.25 \text{ mJy}$ (equivalent to AB magnitude 16.2). This is slightly brighter than the 1 mJy depth of the FIRST catalog; however, in a visual examination of faint FIRST images, many sources fainter than this appeared to be possibly spurious detections. Above this flux limit, there are about 82 FIRST sources per square degree.

3.2. Positional Matching of Point Sources

We restricted the sample to optical point sources using SDSS automated star–galaxy separation (Section 2.1). Figure 1 shows the distribution of FIRST–SDSS distance for radio–optical (point source) matches. The expected contamination by random matches (evaluated by offsetting the FIRST positions by 1° in right ascension) is also shown. The inset plot shows the estimated completeness (solid line; percentage of physical sources recovered) and efficiency (dotted line; percentage of all matches that are physical) as a function of matching radius. The precise choice of matching radius is a tradeoff between sample completeness and sample contamination. Since we are looking for rare objects, we opted more on the side of decreased

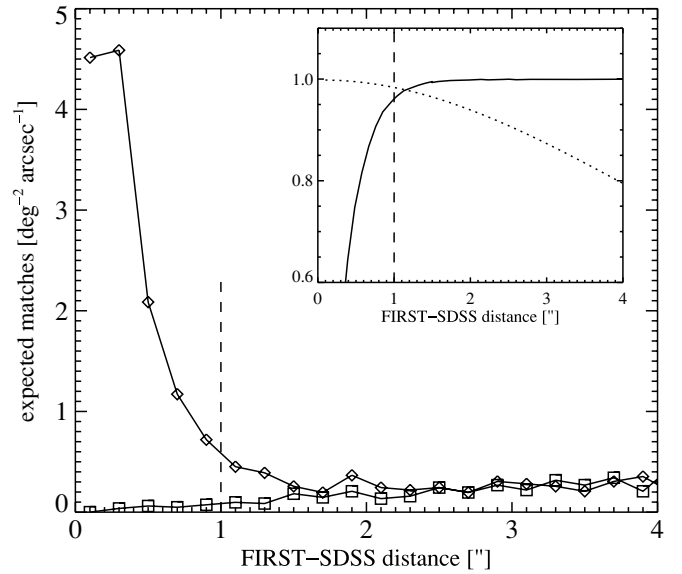


Figure 1. Distribution of FIRST–SDSS distances for FIRST sources matched to SDSS $r < 21$ point sources (diamonds). The level of background contamination (estimated by offsetting positions by 1°) is also shown (squares). The inset plot shows the completeness (solid line) and efficiency (dotted line) as a function of matching radius, estimated by fitting the distance distribution with a simple Gaussian + line model.

contamination and chose to use a $1''$ matching radius. As shown in Figure 1, the matching radius of $1''$ results in 96% completeness and 98% efficiency. There are 2000–3000 SDSS point sources per square degree with $r < 20.5$. Correlating with FIRST positions within $1''$ resulted in $\sim 14,000$ matches.

We did not consider proper motions when matching the two catalogs, but emphasize that this decision should not significantly affect the matching results. All of the observations were performed since 1994. Within the relevant magnitude range, nearly 99% of SDSS stars have an apparent motion of less than $0.1 \text{ arcsec yr}^{-1}$, with a median value of $< 7 \text{ mas yr}^{-1}$. Proper motions⁸ for this sample are much smaller than for the sample of H99 owing to the much fainter flux limit and correspondingly larger source distances.

3.3. Spectral Typing

KI08 showed that a sample of potential radio stars selected by their SDSS colors is strongly contaminated by quasars. There are enough quasars with stellar colors (i.e., within a few hundredths of a magnitude from the main stellar locus in the multi-dimensional SDSS color space) that spectroscopic identifications are necessary in order to cull them from the sample. We therefore required an SDSS spectroscopic observation for each matched source and limited the sample to those with stellar-classified spectra. Of the $\sim 14,000$ selected matches, 6413 have spectra and 292 of those were classified as stellar by the SDSS spectral processing pipeline.

For a more robust determination of spectral type, we executed visual classification of each spectrum. Of the 292 stellar-classified sources, six matched to known quasars (Schneider et al. 2007) and 45 to known BL Lac objects (Plotkin et al. 2008). We removed one object whose spectrum showed broad emission lines signifying the super-position of a star with a quasar. Of course these false matches are not indicative of an

⁸ Proper motions were determined from DR7 of the SDSS following the procedure of Munn et al. (2004).

18% failure rate for the spectral pipeline, which is optimized to detect galaxies, stars, and quasars rather than rare sources such as BL Lac objects. Because the selection criteria for this study are biased toward (radio) quasars, they result in a disproportionately large number of BL Lac objects, which make up a very tiny percentage of the entire SDSS spectroscopic database.

Spectral types were individually assigned to the remaining 240 sources using a custom IDL package dubbed “the Hammer.”⁹ The full algorithm used by the Hammer is described in Appendix A of Covey et al. (2007). In short, the Hammer automatically types input spectra by measuring a suite of spectral indices and performing a least-squares minimization of the residuals between the indices of the target and those measured from spectral type standards. It then allows a confirmation or correction of spectral type according to a *visual* comparison of the input spectrum with spectral templates. Although spectral types are available from the SDSS database, visual confirmation by stellar scientists (authors G.R.K., A.A.W., and J.J.B.) leads to more robust classifications.

With visual classification, the sample was reduced to 194 sources with reliable stellar spectra. The rejected spectra were too noisy for reliable typing or were indicative of BL Lac objects. The latter are not included in the BL Lac sample of Plotkin et al. (2008); their sample was drawn from SDSS Data Release Five (DR5) and thus covers a smaller sky area than the DR6 sample used in this paper.

3.4. Visual Examination of Radio Morphology

We looked at FIRST images of the remaining sample in order to determine the radio morphology of each source. We anticipated that the majority would be point sources, because the resolution of FIRST ($\sim 5''$) is not sufficient to resolve stellar emission. Resolved or multiple-component emission, however, would be strongly indicative of a nonstellar source such as an active galactic nucleus (AGN) with radio jets.

We examined FIRST postage stamps ($2' \times 2'$) and classified each as “compact” (point source emission), “resolved” (resolved single-component emission), “complex” (multiple-component or knotty emission), or “spurious” (e.g., an artifact introduced by interferometric errors). An example from each category is shown in Figure 2. Resolved or complex radio morphology is typically associated with an extragalactic object such as a radio galaxy or quasar.¹⁰ Out of the 194 visually classified images we found six spurious sources, which were removed from the sample. Of the remaining 188 sources, 60 are complex, 16 are resolved, and 112 are compact.¹¹ The high fraction of sources with complex radio emission demonstrates that many radio quasars survived the previous selection criteria. Because these objects clearly show stellar spectra, we interpret them as optically faint radio quasars in chance alignment with bright foreground stars. We rejected the complex sources as obviously extragalactic. However, not all quasars have complex radio emission from detectable lobes, but many are instead point sources (KI08): this is typically thought to be the result of Doppler beaming of a jet aligned along the

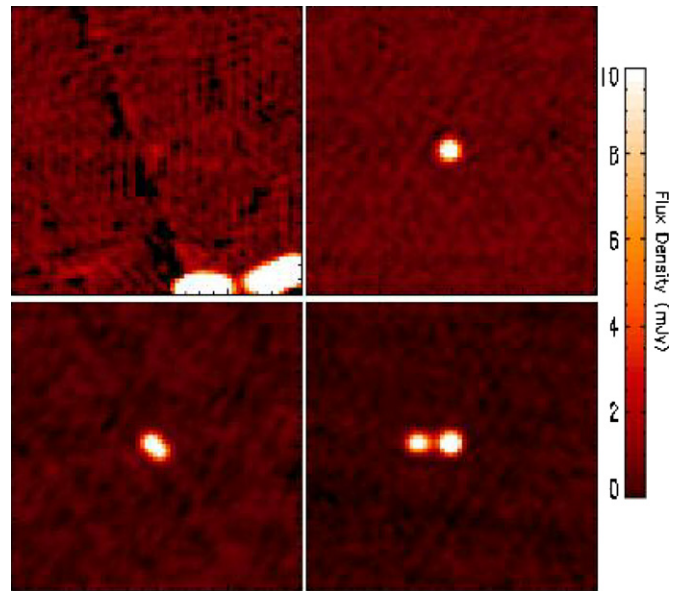


Figure 2. Example FIRST images ($2' \times 2'$) classified by radio morphology as spurious (upper left), compact (upper right), resolved (lower left), and complex (lower right). The position of the optical source is at the center of each image.

(A color version of this figure is available in the online journal.)

line of sight. Thus, despite the thorough visual classifications, the final set of compact radio sources with stellar spectra may remain contaminated by chance star–quasar superpositions. We discuss sample contamination in more detail in Section 3.6.

3.5. Final Sample of Potential Radio Stars

We retain the sample of 112 compact sources for the remaining analysis of this paper. This set of radio star candidates is presented in Table 1, which lists positions, stellar type, radio fluxes, optical magnitudes, and radio morphology classification. The 16 resolved sources and 60 complex sources are listed in Tables 2 and 3, respectively. The tables also list the distance to each star, calculated using the photometric parallax relation of Ivezić et al. (2008a); this relation is valid only for stars on the main sequence. As discussed by Finlator et al. (2000), nearly all SDSS stars ($\sim 99\%$) are expected to lie on the main sequence. However, it is possible that by selecting radio-emitting stars we have biased our sample toward giant stars in the halo (nearby giants are brighter than the $m = 15$ SDSS saturation limit). We note that approximately 40% of the candidate radio stars have $\log(g)$ measured by the SDSS software pipeline; all have $\log(g) > 3$, indicating that they are main-sequence stars. There is no evidence that the sample has a different distance distribution than other SDSS stars with spectra.

Figure 3 is a mosaic of four of the candidate radio sources; it shows the optical image, the radio image, and the optical spectrum for each one. The brightest optical source and the brightest radio source in the sample are included in the mosaic.

3.6. Estimating Sample Contamination

To estimate the contamination originating from chance radio–optical alignments, we created a set of 12 random samples for comparison. To create the random samples, we offset the right ascension or declination in the FIRST catalog (by -1° , $-0^\circ.5$, $-0^\circ.1$, $0^\circ.1$, $0^\circ.5$, or 1°) and then applied identical selection criteria (where possible) as above. The contamination estimate is an upper limit because it is not possible to apply exactly the same selection criteria to the random samples: the SDSS spectral

⁹ <http://www.cfa.harvard.edu/~kcovey/thehammer>

¹⁰ Galactic objects such as H II regions or supernova remnants may show extended emission; however, we do not expect contamination from these sources because our sample is limited to 30° or more above the Galactic plane.

¹¹ For one source that was initially identified as “complex,” the optical image shows a nearby galaxy that appears to be the source of the second point of radio emission. We concluded that the two radio components are physically unrelated and moved that object into the “compact” category, leading to the totals given in the text.

Table 1
Properties of the Radio Star Candidates Sample

SDSS ^a		FIRST ^a		Separation ^b	Distance ^c	Type ^d	Active? ^e	S_{peak}	S_{20}	SDSS Model Magnitudes					4DCD ^f	Catalog
R.A.	decl.	R.A.	decl.	($''$)	(pc)			(mJy beam ⁻¹)	(mJy)	u	g	r	i	z		ID ^g
9.7469648	0.31168685	9.74689	0.31172	0.29	319.640	M2	No	1.93	2.01	21.3	18.8	17.4	16.4	15.9	1.7	55105
27.6658730	-1.13948400	27.66569	-1.13928	0.99	397.880	M2	No	1.82	1.96	21.6	18.9	17.5	16.6	16.2	1.8	155708
44.5010990	1.22593510	44.50115	1.22574	0.73	9830.540	F8	No	11.90	12.40	19.2	18.3	18.1	18.0	18.0	2.8	253325
112.0061000	38.06249000	112.00596	38.06232	0.73	598.000	M1	No	1.44	1.60	22.0	19.8	18.3	17.5	17.1	1.9	612859
114.5806600	48.39231500	114.58059	48.39211	0.76	2750.950	K2	No	1.27	1.81	20.3	18.7	18.1	17.9	17.8	0.8	634578
117.5012900	34.98278400	117.50105	34.98291	0.85	691.950	M1	No	1.83	1.56	21.3	18.9	17.6	17.0	16.6	2.5	660499
117.5527500	24.83105600	117.55283	24.83080	0.96	1139.890	M0	No	2.97	2.85	23.1	19.7	18.4	17.9	17.6	2.2	661031
118.5574000	39.62222400	118.55721	39.62228	0.58	2268.550	F8	No	1.27	1.29	16.9	15.9	15.6	15.5	15.5	0.4	670267
118.6814000	33.29291800	118.68152	33.29275	0.70	515.780	M1	No	1.80	1.93	21.3	18.8	17.4	16.8	16.4	1.1	671427
119.3160100	30.17021500	119.31614	30.17024	0.41	936.480	K4	No	3.57	3.82	19.8	17.7	16.7	16.4	16.2	3.5	677301
119.7809500	17.07585700	119.78081	17.07571	0.71	1613.270	M0	No	2.37	1.79	23.2	20.2	18.9	18.4	18.1	1.2	681437
121.2057400	53.11331800	121.20609	53.11341	0.83	1070.120	M3	No	3.81	4.97	22.6	21.1	19.8	18.8	18.3	3.7	694900
121.3575900	33.92661500	121.35767	33.92649	0.51	1040.680	M3	No	1.74	1.25	23.6	21.6	20.2	19.2	18.6	1.2	696337
122.0831300	40.20902400	122.08297	40.20927	0.99	12403.900	K0	No	1.48	1.36	20.2	19.2	18.9	18.8	18.8	1.2	703419
122.4434000	15.34121000	122.44323	15.34111	0.69	795.440	M2	Yes	1.45	3.43	22.8	20.2	18.9	18.0	17.5	1.9	706934
122.5364400	39.29135700	122.53619	39.29131	0.72	887.850	K4	No	4.99	4.27	18.4	16.6	15.9	15.7	15.6	1.1	707887
123.5006500	29.96177800	123.50080	29.96161	0.77	535.690	M4	Maybe	6.21	5.72	23.0	21.6	20.2	18.8	18.1	2.0	717543
123.5311000	7.57838460	123.53087	7.57825	0.94	395.760	M4	No	1.01	1.58	23.6	20.8	19.3	18.1	17.4	2.4	717871
123.8783600	27.77808900	123.87866	27.77810	0.97	4003.250	G2	No	2.84	2.45	19.5	18.3	17.9	17.8	17.7	1.9	721293
124.0573700	17.92303000	124.05750	17.92286	0.76	1131.870	K4	No	1.38	1.88	19.2	17.4	16.7	16.4	16.3	1.2	723055
125.2091100	42.31718800	125.20885	42.31716	0.69	192.380	M1	No	4.34	4.27	19.7	17.1	15.7	14.9	14.5	0.8	734833
126.3005300	17.33529000	126.30050	17.33502	0.98	1258.650	M1	No	2.15	1.86	23.1	20.8	19.4	18.7	18.4	1.3	746124
127.3762300	47.77290800	127.37631	47.77266	0.92	1149.710	K4	No	194.00	203.00	19.9	17.9	17.1	16.7	16.6	1.4	756772
128.4548800	28.86214000	128.45489	28.86231	0.61	315.370	M3	No	9.40	9.77	22.1	19.7	18.4	17.1	16.5	2.4	767820
129.9784600	17.21355300	129.97861	17.21342	0.69	483.870	M4	Yes	2.50	2.46	23.2	21.6	20.2	18.8	18.0	2.4	783928
131.7995200	8.87368060	131.79954	8.87363	0.20	1409.130	K3	No	1.67	1.89	19.9	17.9	17.2	16.9	16.8	1.2	803383
132.3854500	39.56273500	132.38580	39.56271	0.98	638.660	M0	No	1.43	2.29	21.6	18.9	17.6	17.0	16.7	1.0	809871
133.7192300	22.38336800	133.71919	22.38349	0.46	3791.930	F8	No	3.15	3.00	18.2	17.2	16.9	16.8	16.8	0.3	824171
133.9574700	16.77287300	133.95775	16.77288	0.95	2133.210	G3	No	16.20	17.10	17.6	16.5	16.1	16.0	16.0	2.9	826748
138.3544300	16.92733700	138.35438	16.92730	0.22	930.940	M2	No	4.84	4.56	22.5	20.4	19.1	18.3	17.8	2.6	874572
139.0118400	30.04233700	139.01158	30.04221	0.93	541.220	M4	Yes	2.16	2.39	23.2	21.4	19.9	18.7	18.0	1.3	881748
139.3560700	10.26608300	139.35585	10.26599	0.85	1857.790	M0	No	5.43	5.64	23.1	20.7	19.4	18.9	18.5	1.6	885740
141.1869700	0.31937489	141.18692	0.31913	0.90	1303.670	K7	No	2.02	1.73	21.3	18.9	17.9	17.4	17.2	2.8	905754
141.6470700	57.00886200	141.64733	57.00864	0.95	279.810	M3	No	2.52	2.32	21.5	18.9	17.6	16.4	15.8	2.5	910742
143.3109900	12.15141900	143.31114	12.15164	0.96	2456.660	F8	No	2.07	2.39	17.9	16.8	16.4	16.3	16.3	0.6	928953
146.3638800	9.77656370	146.36362	9.77655	0.92	3746.860	G0	No	1.82	1.79	19.2	18.0	17.7	17.5	17.5	0.3	961831
146.4080800	26.34171200	146.40830	26.34187	0.91	579.290	M1	No	1.48	1.46	23.7	19.8	18.3	17.6	17.2	3.9	962290
149.2323800	52.95324400	149.23257	52.95304	0.84	508.330	M3	No	1.47	1.67	23.2	20.6	19.1	18.1	17.5	1.9	992960
149.6155300	28.79923000	149.61566	28.79928	0.44	187.950	M3	No	1.03	1.33	21.6	18.8	17.4	16.2	15.5	0.9	997266
150.4368400	27.94595600	150.43664	27.94598	0.65	566.560	M2	No	1.01	1.30	21.8	19.4	18.0	17.2	16.7	1.5	1006282

Notes. The table of 112 candidate radio stars is available in the electronic version of this paper, and is also downloadable from <http://www.astro.washington.edu/users/akimball/radiocat/radiostars/>.

^a Right ascension and declination are given in decimal degrees.

^b Offset between FIRST and SDSS positions.

^c Distance was determined using the photometric parallax relation of Ivezić et al. (2008a); the relation is valid only for stars on the main sequence.

^d Visually confirmed spectral classification.

^e A “yes” indicates a spectrum with reliable H α emission.

^f Four-dimensional color distance from the stellar locus, defined in Section 4.1 of the text.

^g Internal ID of the source in the radio catalog of KI08.

(This table is available in its entirety in a machine-readable form in the online journal. A portion is shown here for guidance regarding its form and content.)

target selection for quasars (Section 2.1) ensures that a large fraction of the real FIRST–SDSS matches have spectral data, whereas very few sources in the random samples have SDSS spectra.

Having performed the matching several times, we can determine the variance of the random sampling.¹² Random match-

ing of all FIRST and photometric SDSS sources resulted in 3242 ± 65 matches. Applying the r magnitude and radio flux limits reduced the samples to 759 ± 30 matches. Selecting on optical point source morphology further reduced the samples to 422 ± 20 .

The next selection step for the real sample was to eliminate those sources without SDSS spectra. The equivalent step for the random samples is to eliminate those that could not have qualified for SDSS spectral targeting. The quasar targeting

¹² Varying the FIRST positions results in a slight decrease of the areal overlap between FIRST and SDSS. However, given that so few matches result from the random sampling, the small change in the matching area has no significant effect on the contamination estimate.

Table 2
“Candidate Radio Stars” with Resolved Radio Emission

SDSS ^a		FIRST ^a		Separation ^b (")	Distance ^c (pc)	Type ^d	Active? ^e	S_{peak} (mJy beam ⁻¹)	S_{20} (mJy)	SDSS Model Magnitudes					Catalog	ID ^g
R.A.	decl.	R.A.	decl.							u	g	r	i	z		
123.1976100	20.64439200	123.19768	20.64418	0.80	351.420	M1	No	1.25	2.11	20.6	18.0	16.6	15.9	15.5	0.6	714327
129.6339900	13.72514400	129.63398	13.72527	0.45	2147.920	G4	No	16.60	30.00	18.4	17.2	16.7	16.6	16.5	4.6	780377
159.1123200	12.80009800	159.11230	12.80003	0.26	12229.900	F7	No	68.30	103.00	20.2	19.3	19.1	19.0	18.9	3.5	1101138
179.5614700	37.07555200	179.56123	37.07574	0.97	6233.260	K2	No	1.39	2.07	21.7	20.4	19.8	19.6	19.4	1.6	1324909
179.9687500	44.91827900	179.96864	44.91834	0.36	6285.120	G5	No	3.73	6.41	20.4	19.5	19.1	18.9	18.8	3.1	1329461
183.0861100	27.54304500	183.08620	27.54281	0.89	687.640	M2	No	4.66	7.81	23.2	20.3	18.8	18.0	17.5	0.8	1363672
189.3334100	53.88457500	189.33319	53.88464	0.52	2723.890	G1	No	3.37	6.85	18.8	17.7	17.2	17.1	17.0	2.2	1431967
198.7216200	10.62265900	198.72157	10.62287	0.78	1404.190	M2	No	3.75	7.46	22.8	21.2	19.9	19.1	18.4	5.6	1534251
217.8390300	8.53663970	217.83908	8.53640	0.88	2057.150	K4	No	1.92	4.61	21.1	19.1	18.3	17.9	17.8	1.0	1742370
228.9030100	6.33068160	228.90314	6.33059	0.56	2877.940	G1	No	2.90	5.90	18.3	17.4	17.0	16.9	16.8	3.0	1863654
240.3610400	9.07629920	240.36122	9.07639	0.72	1297.210	M1	No	30.30	62.30	23.4	20.5	19.2	18.5	18.2	0.5	1985947
241.6174600	32.45298600	241.61725	32.45302	0.65	934.290	M1	No	13.60	26.00	22.1	19.7	18.5	17.7	17.3	3.4	1998928
251.0205900	26.75291400	251.02068	26.75277	0.60	9124.150	F8	No	3.67	7.14	19.9	18.9	18.7	18.5	18.5	2.8	2089662
253.7596800	32.12100800	253.75963	32.12106	0.24	1440.760	K4	No	1.02	4.60	21.2	19.1	18.0	17.6	17.4	1.7	2113922
254.7470100	23.40834500	254.74695	23.40835	0.21	548.530	M0	Yes	1.27	2.70	20.7	18.6	17.3	16.6	16.2	3.9	2122609
258.2688900	32.22357000	258.26875	32.22338	0.81	2846.860	F9	No	1.44	3.51	18.2	17.2	16.9	16.7	16.7	3.0	2152684

Notes. The table of 16 sources with resolved radio emission (which passed all other selection criteria) is available in the electronic version of this paper, and is also downloadable from <http://www.astro.washington.edu/users/akimball/radiocat/radiostars/>.

^a Right ascension and declination are given in decimal degrees.

^b Offset between FIRST and SDSS positions.

^c Distance was determined using the photometric parallax relation of Ivezić et al. (2008a); the relation is valid only for stars on the main sequence.

^d Visually confirmed spectral classification.

^e A “yes” indicates a spectrum with reliable H α emission.

^f Four-dimensional color distance from the stellar locus, defined in Section 4.1 of the text.

^g Internal ID of the source in the radio catalog of KI08.

(This table is also available in a machine-readable form in the online journal.)

algorithm (Section 2.1) depends on the proximity to a radio source; by artificially shifting the FIRST positions to create the random samples, we created fake optical–radio sources that would pass the selection criteria. We rejected sources outside of the DR6 spectroscopic coverage, which is smaller than the DR6 photometric coverage. Keeping only those matches that would qualify for SDSS spectroscopy reduced the random samples to 225 ± 22 . Applying the success rate of spectral sampling of SDSS targets (92.5%; Blanton et al. 2003) results in an expected random sample size of 208 ± 20 .

We can make an educated guess that the remaining random samples consist almost entirely of stars: at these very bright magnitudes, the SDSS star–galaxy separation mechanism is quite effective at differentiating between point sources and extended sources. Besides stars, the most common type of optical point source is a quasar, but these are rare at $i < 19.1$. For example, the highest fraction of quasars in the SDSS can be found at the north Galactic pole, where there are about 100 stars for each quasar (at magnitudes $i < 19$; Jurić et al. 2008). Close to the Galactic plane, the quasar fraction is much smaller.

The final step in the selection process was to visually classify each source according to its radio morphology. Only those objects that appeared by eye to be unresolved in their FIRST image were retained. Selecting these objects results in a random sample size of 117 ± 14 . Applying the spectral observation success rate reduces that value to 110 ± 14 . Estimating that 1% of the sample are quasars as described above, the final estimate is 108 ± 13 . This number is essentially identical to the size of the candidate radio stars sample, which consists of 104 stars from DR6 and 8 additional stars with spectroscopy performed later than that of DR6.

The above comparison shows that most or all of the potential radio stars are actually chance alignments of SDSS stars with unrelated FIRST sources. The variance in the random samples is large enough that there may be several real radio stars in the candidates sample or none at all. This result indicates that radio stars are extremely rare or nonexistent in the range $15 < i < 19.1$, $S_{20} < 1.25$ mJy.

3.7. The Fraction of Radio Stars in the SDSS

We can use the relative sizes of the candidate and random samples, along with the sample completeness, to calculate an upper limit on the fraction of radio stars in the SDSS. The candidate sample contains 104 stars with spectra in DR6; 98 of those are in the magnitude range $15 < i < 19.1$. As discussed previously, the estimated number of contaminating sources is 108 ± 13 . We can therefore state with 97.5% confidence that there are no more than 16 radio stars in the sample of candidates (using the one-sided 2σ error estimate). The completeness estimate has the following contributions: (1) the completeness of the FIRST survey at 1.25 mJy is approximately 85%–90% (Becker et al. 1995); (2) the completeness of the radio–optical matching within 1" is 96%; (3) the SDSS spectroscopic targeting algorithm selects all $15 < i < 19.1$ objects within 2" of a FIRST source (100% completeness); and (4) given fiber collisions, the success rate of spectroscopic observations is about 92.5%¹³ (Blanton et al. 2003). We therefore estimate that the sample is about 75% complete, and thus that there are no more than 21 radio stars in

¹³ The success rate is not biased with respect to the radio sample; we verified that approximately 92.5% of our selected sources that should have passed the targeting selection do in fact have SDSS spectra.

Table 3
 “Candidate Radio Stars” with Complex Radio Emission

SDSS ^a		FIRST ^a		Separation ^b	Distance ^c			S_{peak}	S_{20}	SDSS Model Magnitudes					Catalog	
R.A.	decl.	R.A.	decl.	($''$)	(pc)	Type ^d	Active? ^e	(mJy beam ⁻¹)	(mJy)	u	g	r	i	z	4DCD ^f	ID ^g
8.8779417	-10.33142200	8.87798	-10.33148	0.25	365.070	M3	No	4.87	5.79	22.6	19.7	18.3	17.2	16.6	0.7	50158
16.4108070	0.04541176	16.41080	0.04553	0.43	1605.120	K7	No	1.36	4.61	22.9	20.3	19.0	18.5	18.3	3.2	92777
30.9980570	-9.00080110	30.99826	-9.00074	0.75	1409.850	G2	No	1.41	1.97	16.7	15.6	15.2	15.1	15.1	0.4	174929
31.6274380	-8.36097310	31.62769	-8.36088	0.96	7284.830	F8	No	1.05	1.96	20.0	19.0	18.6	18.5	18.5	1.3	178794
115.4349200	33.59706800	115.43505	33.59718	0.57	660.370	M3	No	117.00	137.00	23.3	20.8	19.3	18.3	17.8	0.5	642007
116.5239800	33.14653100	116.52415	33.14652	0.51	1299.940	G5	No	24.40	42.50	17.2	16.0	15.6	15.5	15.4	0.8	651724
118.6515700	31.04799200	118.65183	31.04788	0.89	976.060	K2	No	3.14	5.70	18.2	16.6	15.9	15.7	15.6	1.1	671131
120.2777900	31.98149700	120.27754	31.98134	0.95	3123.470	G5	No	1.40	1.80	18.7	17.5	17.2	17.0	17.0	1.1	686143
122.4168500	9.98404330	122.41704	9.98402	0.69	2606.500	G8	No	9.55	22.70	19.4	18.1	17.6	17.4	17.3	1.1	706655
125.7096000	12.55254200	125.70952	12.55259	0.33	857.030	M3	Yes	7.58	15.40	23.0	21.4	19.9	19.0	18.5	4.2	740037
128.9825100	32.53530500	128.98271	32.53522	0.69	919.880	F8	No	29.40	53.70	23.7	22.6	21.0	19.9	19.3	3.5	773185
131.5889500	13.51593600	131.58898	13.51595	0.10	881.950	M3	Maybe	4.53	6.21	23.3	21.4	20.0	18.9	18.4	1.3	801062
131.9006900	15.72048400	131.90071	15.72021	0.99	916.410	M3	No	1.08	3.20	22.6	21.5	20.0	19.1	18.6	3.7	804509
132.1393200	3.49329870	132.13913	3.49330	0.69	7584.010	M2	No	5.51	13.10	20.3	19.4	19.0	18.9	18.9	2.7	807208
133.3787500	3.04040040	133.37881	3.04044	0.27	1017.230	M1	No	5.67	8.47	22.9	20.4	19.1	18.3	17.9	0.7	820636
134.9379600	15.68712000	134.93808	15.68694	0.77	1733.890	K4	No	29.40	32.10	21.0	19.0	18.1	17.7	17.6	1.6	837341
135.5234500	-0.30775603	135.52351	-0.30753	0.84	1238.090	K7	No	2.59	3.77	21.8	19.4	18.2	17.7	17.5	1.1	843673
140.7074600	0.98319174	140.70767	0.98337	0.98	2584.960	K2	No	10.50	16.70	19.6	18.3	17.7	17.5	17.4	1.6	900871
141.8337800	14.43029200	141.83377	14.43037	0.28	392.550	M4	No	10.60	11.40	22.6	20.4	19.0	17.7	17.1	1.3	912857
147.9741100	0.86803458	147.97390	0.86804	0.76	426.410	M4	Yes	5.80	7.25	22.7	20.6	19.2	17.9	17.2	2.1	979415
148.9287500	40.24028700	148.92868	40.24017	0.46	301.060	M4	No	2.90	5.75	22.6	20.2	18.8	17.4	16.7	1.2	989703
153.7401400	14.70054700	153.74037	14.70052	0.80	1375.330	K7	No	7.83	11.60	21.7	19.2	18.1	17.6	17.4	1.6	1042751
154.0058700	12.36168900	154.00611	12.36181	0.95	2299.170	K7	No	7.56	8.66	22.4	20.2	19.1	18.7	18.5	2.0	1045679
160.5310600	3.99054340	160.53126	3.99068	0.88	809.980	M3	No	5.64	8.20	23.0	21.3	20.0	18.9	18.2	2.6	1116725
172.0590700	21.93210400	172.05921	21.93225	0.71	602.870	M4	No	4.60	6.45	23.9	21.6	20.3	18.9	18.2	2.3	1242017
178.5105200	3.21151700	178.51063	3.21162	0.54	10917.700	F4	No	54.30	72.20	19.9	19.0	18.7	18.7	18.7	1.1	1313182
186.8444200	46.53642400	186.84434	46.53632	0.42	2233.410	M0	No	8.41	14.90	22.5	20.6	19.5	18.9	18.5	5.0	1404584
190.8415000	46.59573600	190.84160	46.59557	0.64	2809.610	G5	No	1.06	3.81	18.9	17.8	17.3	17.2	17.1	2.6	1448337
192.3993900	56.38570800	192.39941	56.38545	0.93	725.890	M3	No	3.69	7.14	24.3	21.6	20.2	19.0	18.4	1.2	1464807
193.9675000	31.88372100	193.96775	31.88354	0.99	210.780	M3	No	4.00	4.35	21.4	18.7	17.3	16.2	15.6	0.1	1481709
197.6279900	33.34007600	197.62815	33.34020	0.67	10157.700	F8	No	4.35	10.40	20.5	19.5	19.2	19.1	19.0	2.2	1522015
201.2052100	5.60704680	201.20533	5.60704	0.41	1180.150	M3	Yes	62.40	86.40	23.0	21.5	20.1	19.1	18.5	3.7	1560947
202.4219100	15.17273900	202.42210	15.17276	0.65	4081.440	G1	No	2.03	1.64	19.8	18.6	18.1	18.0	18.0	0.9	1574101
205.6391100	5.67827170	205.63935	5.67824	0.87	2825.760	K3	No	4.67	12.30	21.2	19.3	18.6	18.3	18.3	2.7	1609487
210.7047200	12.91670100	210.70454	12.91681	0.73	1779.550	G8	No	39.60	66.90	19.0	17.5	16.9	16.7	16.7	1.1	1664852
217.6153300	28.86087300	217.61540	28.86071	0.62	595.960	M4	No	4.96	8.91	23.2	21.7	20.3	19.0	18.4	2.4	1739974
218.2539000	0.91080436	218.25392	0.91101	0.74	5947.670	G3	No	6.10	43.80	20.1	19.1	18.7	18.5	18.5	2.6	1747053
224.7479200	28.45951200	224.74793	28.45956	0.18	5931.480	G6	No	3.09	4.70	20.2	19.2	18.8	18.6	18.6	1.1	1818456
226.8208200	23.24544500	226.82090	23.24539	0.34	1367.660	K5	No	2.97	7.14	21.5	19.1	18.0	17.6	17.3	0.8	1841133
227.4059200	0.57614608	227.40614	0.57622	0.83	581.020	M3	No	3.35	2.96	23.0	19.9	18.6	17.6	16.9	5.2	1847417

Notes. The table of 60 sources with complex radio emission (which passed all other selection criteria) is available in the electronic version of this paper, and is also downloadable from <http://www.astro.washington.edu/users/akimball/radiocat/radiostars/>.

^a Right ascension and declination are given in decimal degrees.

^b Offset between FIRST and SDSS positions.

^c Distance was determined using the photometric parallax relation of Ivezić et al. (2008a); the relation is valid only for stars on the main sequence.

^d Visually confirmed spectral classification.

^e A “yes” indicates a spectrum with reliable H α emission.

^f Four-dimensional color distance from the stellar locus, defined in Section 4.1 of the text.

^g Internal ID of the source in the radio catalog of KI08.

(This table is available in its entirety in a machine-readable form in the online journal. A portion is shown here for guidance regarding its form and content.)

the SDSS DR6 with $15 < i < 19.1$. There are approximately 18 million SDSS stars in this magnitude range, which implies that no more than 1.2 out of every million stars in the range $15 < i < 19.1$ have a radio flux of $S_{20} \geq 1.25$ mJy. For stars with $i \approx 15$, this corresponds to an upper limit on radio-to-optical flux ratio of 0.34; for the $i \approx 19.1$ stars at the faint end, the upper limit on radio-to-optical flux ratio is 15.

4. OPTICAL PROPERTIES

We showed in the previous section that the sample is highly contaminated by interloping AGN. However, statistical comparisons of the sample with typical stars can highlight the most likely actual radio stars. In this section, we examine optical properties of the sample: photometric colors, distance from

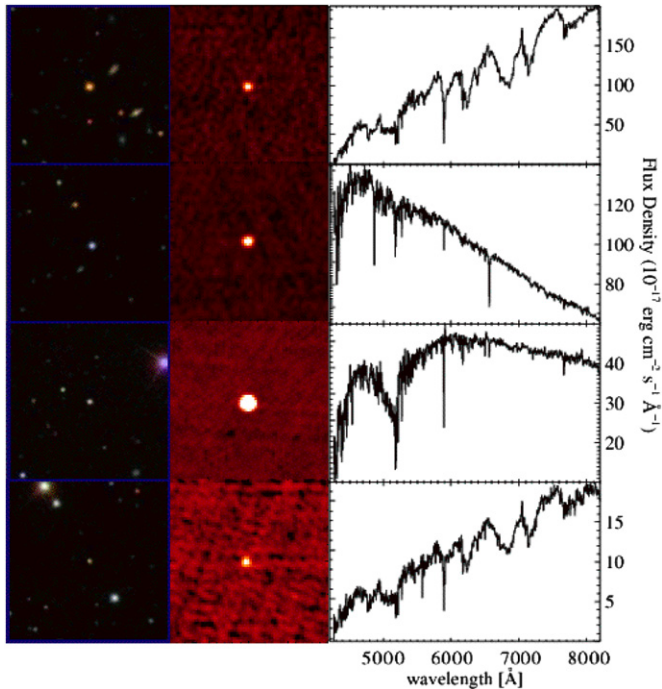


Figure 3. Data for four of the FIRST–SDSS star matches. The left column shows the optical image ($2' \times 2'$), a composite of the g -, r -, and i -band images; the middle column shows the FIRST image ($2' \times 2'$) with linear scaling; the right column shows the SDSS spectrum (F_λ). The top row shows the brightest optical source, an M1 dwarf with $i = 14.9$ and $S_{20} = 4.3$ mJy. The second row shows a G3 dwarf with $i = 16.0$ and $S_{20} = 17.1$ mJy. The third row shows the brightest radio source, a K4 dwarf with $i = 16.7$ and $S_{20} = 203$ mJy. The bottom row shows an M1 dwarf with weak $H\alpha$ emission (not visible on the scale of this figure), $i = 17.8$ and $S_{20} = 6.6$ mJy.

(A color version of this figure is available in the online journal.)

the stellar locus, spectral type, and magnetic activity. We also use an *SDSS control sample* selected from a strip of sky 1° wide in right ascension. The control sample contains point sources with $15 < i < 19.1$ and $r < 20.5$ from the region $236 < \text{R.A.} < 237$, $-2.5 \lesssim \text{decl.} \lesssim 65$; it contains just over 160,000 sources.

4.1. Photometric Colors

Figure 4 presents the distribution of the candidate radio stars in optical color–color space, compared to the SDSS stellar locus as parameterized by Covey et al. (2007). The majority of the candidate stars lie on the stellar locus. Several stars, however, appear to lie along the white-dwarf–M dwarf (WD+dM) bridge (Smolčić et al. 2004): $u - g < 2$, $g - r > 0.3$, $r - i > 0.7$. Such close binary pairs are found to be more active than their single field counterparts (e.g., Silvestri et al. 2005, 2006). Smolčić et al. (2004) limited their analysis to stars with $u < 20.5$ to eliminate those with poor photometry. In the SDSS control sample, less than 0.1% of stars lie on the WD+dM bridge. The candidate radio stars sample contains seven stars that lie along the WD+dM bridge, corresponding to a much higher fraction. We however note that all of our WD+dM candidates have u -band magnitudes > 20.5 ; therefore u -band photometry may have artificially moved these sources blueward of the M star locus (upper right corner of the stellar locus). None of their spectra suggest the presence of a white dwarf companion. We note that the star with $u - g < 0$ is not on the WD+dM bridge, as it has $r - i \sim 0.15$. However, the spectrum and photometric image do suggest that it is a (physical or optical) binary system: a K3 star with an added blue component.

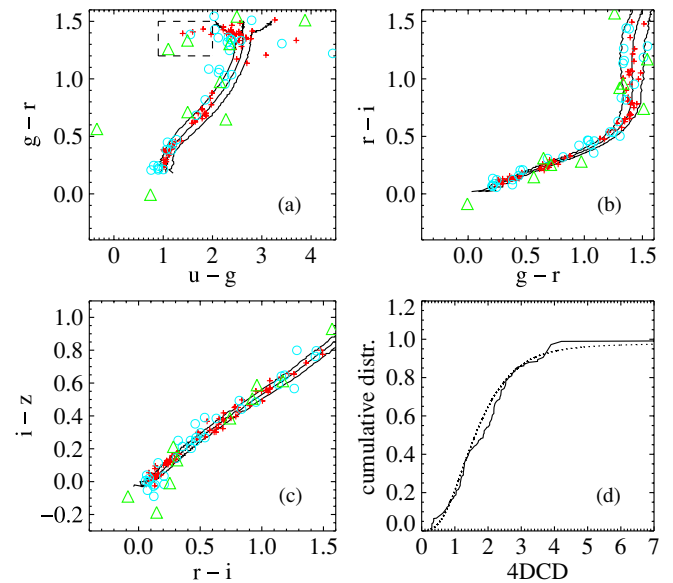


Figure 4. Outliers from the stellar locus. Panels (a)–(c): color–color diagrams with potential radio stars plotted as symbols. The red plus signs indicate candidate radio stars consistent with being on the stellar locus, having $4\text{DCD} < 2$ (see text and Equation (1) for definition); cyan circles indicate those with $2 < 4\text{DCD} < 3$; green triangles indicate those with $3 < 4\text{DCD}$. The dashed-line rectangle in panel (a) surrounds the stars with WD+dM bridge colors. The SDSS stellar locus is shown by the solid lines, as parameterized by Covey et al. (2007). The three lines indicate the position of the stellar locus and its interquartile width, projected onto two dimensions. Panel (d): cumulative distributions of 4DCD for the candidate radio stars sample (solid line) and for the SDSS control sample (dotted line).

(A color version of this figure is available in the online journal.)

A quantitative method of finding outliers from the stellar locus, taking photometric errors into account, is outlined by Covey et al. (2007). They parameterized the stellar locus by finding its 1σ width in the standard SDSS colors ($u - g$, $g - r$, $r - i$, $i - z$) and Two-Micron All Sky Survey (Skrutskie et al. 2006) colors as a function of $g - i$. They chose $g - i$ as the fiducial color because it samples the largest wavelength range possible without relying on the shallower u or z measurements. Using only the SDSS colors, we define a “four-dimensional color distance” (4DCD; analogous to the seven-dimensional version discussed in C07¹⁴), which describes the statistical significance of the distance in color space between a target object and the point on the stellar locus with the same $g - i$ color as the target. The 4DCD is defined by

$$4\text{DCD} = \left[\sum_{k=0}^3 \frac{(X_k^{\text{target}} - X_k^{\text{locus}})^2}{\sigma_X^2(\text{locus}) + \sigma_x^2} \right]^{1/2}, \quad (1)$$

where $X_0 = u - g$, $X_1 = g - r$, etc. The width of the stellar locus is $\sigma_X(\text{locus})$, which refers to the FWHM of the locus in color X_k at the same $g - i$ as the target object. The error in the target’s color, σ_x , is calculated by adding in quadrature its photometric errors in the two appropriate filters.

We characterize outliers from the stellar locus as those with a value of 4DCD greater than 2, shown as circles in Figure 4. Extreme outliers, with $4\text{DCD} > 3$, are shown as triangles. Three of the stars with WD+dM colors have $4\text{DCD} > 2$; these are strong candidates for further investigation. The lower right

¹⁴ Our definition differs from C07 by a square root operator, such that our value is in the units of a color distance.

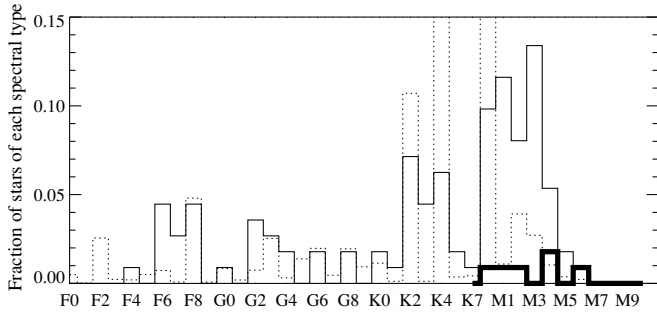


Figure 5. Spectral types of the candidate radio stars (solid line). The thick line indicates the six stars with $H\alpha$ in emission. SDSS stars with $15 < i < 19.1$ and $r < 20.5$ are also shown (dotted line).

panel compares the cumulative distributions for the candidate radio stars (full line) and the SDSS control sample; the two distributions are similar. The largest 4DCD value of ~ 14 belongs to the possibly binary star mentioned earlier, having $u - g < 0$. The other most extreme outlier has 4DCD ~ 6.4 . The spectrum of this object also shows some evidence that the source is part of a multiple system, such as the super-position of a late-type with an early type M star. All other values of 4DCD are < 4.3 .

4.2. Spectral Type and Activity Fraction

Because nonthermal radio emission is a signal of activity, we expect that radio emission may correlate with strong spectral lines, such as $H\alpha$, which are also known to signal magnetic activity. We investigate the fraction of active stars in our sample; if the sample contains some real radio stars which are active, we may see an increase over the active fraction of *all* stars (without selecting for radio emission). Previous studies have found that the fraction of active M dwarfs is a strong function of spectral type (West et al. 2004, 2008), tending to increase toward later subtypes with a peak around M8 dwarfs.

An $H\alpha$ equivalent width was measured for each stellar spectrum using the Hammer (Section 3.3). As discussed by West et al. (2008), the accuracy of such measurements has been tested via Monte Carlo simulations to ascertain how well line strength can be determined at a given S/N level. The $H\alpha$ emission can be recovered over 96% of the time for all spectral types. Figure 5 shows the spectral types of the candidate radio stars sample (solid line), compared with all SDSS DR6 stars with spectra (just under 1 million stars; dotted line). Spectral types for the SDSS sample come from the automated version of the Hammer, while spectral types for the candidate radio star sample were visually confirmed (Section 3.3). Automated Hammer classifications are typically accurate to within ± 4 subtypes for A–G stars and within ± 2 subtypes for K and M stars (Covey et al. 2007). All spectra for the radio stars sample have S/N greater than 2.9. As shown in Figure 5, all of the active candidate radio stars are M dwarfs. This is not a surprising result given that most stars are M dwarfs (Covey et al. 2008; Bochanski et al. 2009), and the majority of activity in main-sequence stars is seen in M dwarfs (e.g., Gizis et al. 2002). West et al. (2008) discussed the fraction of active M dwarfs in SDSS DR5 as a function of spectral subtype, after removing WD+dM bridge stars from their sample. They found that M0–M3 stars have an active fraction of roughly 5%–20%, and that the fraction increases strongly for M dwarfs of later subtype. Our results for the candidate radio stars are consistent with the results of that study for all stars; we do not see a significantly higher fraction of active stars in the sample of candidate stellar radio sources.

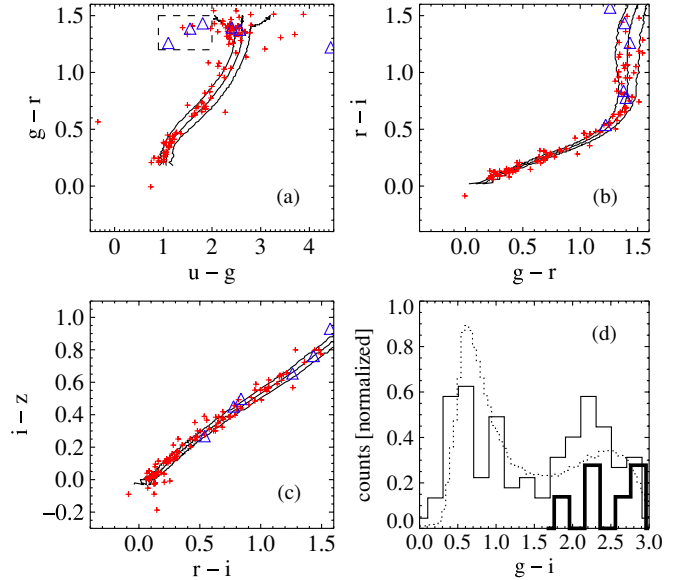


Figure 6. Activity in the candidate radio stars sample. Panels (a)–(c): color–color diagrams with the inactive stars indicated by red plus signs and the active stars (showing $H\alpha$ in emission) indicated by blue triangles. The dashed-line square in panel (a) surrounds the stars with WD+dM bridge colors. The SDSS stellar locus is shown by the solid lines, as parameterized by Covey et al. (2007). The three lines indicate the position of the stellar locus and its interquartile width, projected onto two dimensions. Panel (d): the thin solid line shows the distribution of $g-i$ for the candidate radio stars with $i < 19.1$. The thick line indicates the six active stars. The dotted line corresponds to stars in the SDSS control sample with photometric errors less than 0.1 mag in g and i .

(A color version of this figure is available in the online journal.)

Figure 6 shows color–color diagrams of the candidate radio stars and the SDSS control sample, with the six active stars indicated by triangles. Three of the seven stars with WD+dM bridge colors (Section 4.1) are active; two of these are outliers from the stellar locus (4DCD > 2). This result is in agreement with Silvestri et al. (2006), who suggested that 20%–60% of all WD+dM binaries are magnetically active. The lower right panel of Figure 6 shows the $g-i$ distribution of the SDSS control sample (dotted line), the candidate radio stars (thin solid line), and the active stars (thick solid line). Covey et al. (2007) showed that $g-i$ correlates strongly with the stellar spectral type. The distribution is bimodal in flux-limited samples: it is biased toward red stars, which are the most common, but also blue stars, which can be seen from much greater distances. West et al. (2004) and Bochanski et al. (2007) compared the colors of active to inactive M dwarfs in the field (i.e., not part of a binary system). They found no significant differences between the two populations. The current radio stars study includes three active field M dwarfs (i.e., M dwarfs that do not have WD+dM bridge colors). Although the sample is too small to make a strong statement in comparison with the studies of West et al. (2004) and Bochanski et al. (2007), we note that our results for stars with radio emission are consistent with their conclusions for all stars.

5. RADIO PROPERTIES

5.1. Radio Spectral Slope

Using the multiple-wavelength radio catalog presented by KI08, we find that eight of the candidate radio stars were detected in a second radio sky survey: either at 92 cm in WENSS or at 6 cm in GB6 (or both). We can therefore determine the

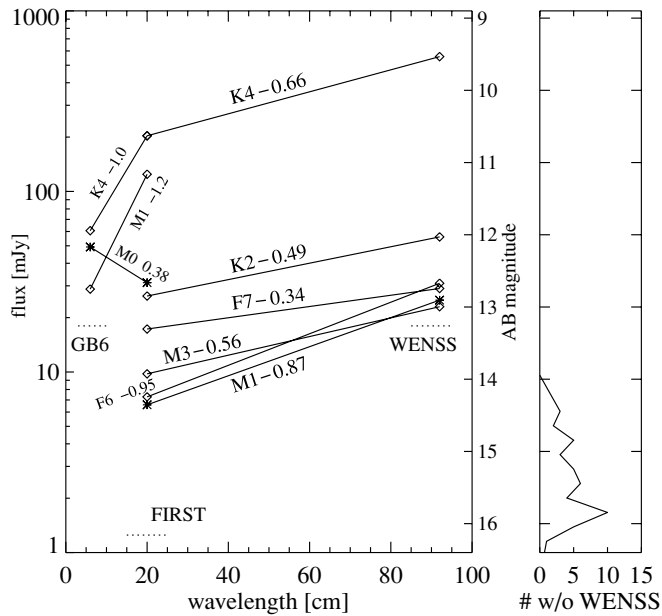


Figure 7. Left: radio spectra of the candidate radio stars detected at more than one radio wavelength. Diamonds indicate inactive stars and asterisks indicate active stars. The visually confirmed spectral type and the power-law index are labeled for each source. Right: distribution of FIRST fluxes for the 44 candidate radio stars which lie in the region of the sky observed by WENSS, but were not detected at 92 cm.

radio spectral index α (where $F_\nu \propto \nu^\alpha$), and we report those results here. We compare the results with samples of the type of AGN that may be contaminating the sample (Section 3.6).

The value of the spectral index is a clue about the environment at the source of emission. Nonthermal radio emission is typically due to synchrotron (relativistic) or gyrosynchrotron (semi-relativistic) electrons accelerating in a magnetic field. Synchrotron and gyrosynchrotron processes result in a negative spectral slope ($\alpha \sim -0.8$) in the optically thin case, and a flat or positive slope in the optically thick case. Such emission has been detected from M dwarfs in both their flaring (rapidly variable) and quiescent (nonflaring) states (e.g., Güdel & Benz 1996; Large et al. 1989; Bastian & Bookbinder 1987; Osten et al. 2006).

Fifty stars in our sample lie within the WENSS sky coverage and 106 lie within the GB6 sky coverage. Following KI08, we use $30''$ as the FIRST–WENSS matching radius and $70''$ as the FIRST–GB6 matching radius. These choices result in estimates of 99% completeness with 92% efficiency (WENSS) and 98% completeness with 79% efficiency (GB6; see Table 2 of KI08). Six sources have 92 cm detections and three have 6 cm detections; only one source was detected at all three wavelengths. FIRST is much deeper than WENSS or GB6; therefore, only sources that are very bright or have very steep spectral slopes can be detected in more than one survey. Despite the poorer positional accuracy of GB6 and WENSS, these matches are highly reliable because of their lower source sky density.¹⁵ Figure 7 presents the radio spectra of these sources. Four of the stars are M dwarfs, two of which are active (Section 4.2).

From the KI08 catalog, we selected a sample of AGN using the radio criteria that were applied to the radio stars sample: $S_{20} \leq 1.25$ mJy, unresolved in FIRST (using Equation 3 of

KI08), and a WENSS match within $30''$. These criteria select the type of objects that could be contaminating the sample of potential radio stars discussed in this section. The stellar sample has a similar spectral slope distribution to the AGN sample, whose median (mean) spectral index is -0.67 (-0.54). The spectral slope distributions do not allow a definitive conclusion as to whether any of the candidate radio stars with multiple radio detections are actual radio stars or are contaminating AGNs.

5.2. Variability

It is possible that the radio fluxes varied over the course of observations by the different surveys. Both stellar radio sources and AGNs are known to vary in the radio. For example, Berger (2002) observed variability in the nonflaring radio emission from cool dwarfs over timescales of merely hours. (However, the fluxes in that study were far below the flux limit of the current study.) The likely AGN contaminants are quasar core sources, which are known to vary with timescales ranging from days to years (e.g., Rys & Machalski 1990; Barvainis et al. 2005). About half of the candidate radio stars sample was observed multiple times in FIRST, most with timescales of less than a week. None showed significant variability at 20 cm. We note that nearly half of the radio stars found by H99 varied in FIRST at the 4σ level.

6. CONCLUSIONS

We performed a search for radio stars by combining radio and optical observations from FIRST (20 cm) and SDSS. This is the first large-scale search for radio stars using an optical survey faint enough to include a large number of M dwarfs. Many of these late-type stars are known to be magnetically active. A sample of 112 candidates was selected using the following criteria: optical point source morphology as determined by the SDSS photometric pipeline; radio and optical positions matched within $1''$; an optical magnitude $r < 20.5$ to ensure reliable determination of optical morphology; radio flux $S_{20} \geq 1.25$ to eliminate spurious sources; a spectrum visually classified as stellar; and radio point source morphology. We estimated sample contamination using random matching and similar selection criteria. The size of the random samples (108 ± 13) suggests that the potential radio stars are heavily contaminated by optically faint radio quasars in chance alignment with a foreground star. The main ambiguity in determining radio–optical matches stems from uncertainty as to whether the star is actually the source of the radio emission. It may be possible to overcome this problem with careful follow-up using very long baseline interferometry to determine proper motions of the radio sources.

In Section 3.7, we calculated the upper limit on the fraction of radio stars (with $S_{20} \geq 1.25$ mJy) no more than 1.2 per million stars in the magnitude range $15 < i < 19.1$. We note that some M stars have been observed to occasionally flare brightly in the radio; however, these stars have a very small duty cycle and very few will be detected in a single-epoch survey such as FIRST. While some M dwarfs have been shown to have constant radio emission (e.g., Berger 2002; Osten et al. 2006), it is at much fainter levels than radio emission in their flare state by about an order of magnitude. Our results effectively rule out a population of radio-bright late-type stars.

We compared the candidate sample to SDSS stars in the same magnitude range and investigated their distributions in optical color, stellar type, magnetic activity, and distance from the stellar locus in color–color space. The two data sets show similar distributions. However, there is a higher fraction of

¹⁵ For each object, we verified that the radio star candidate is the nearest FIRST source to the GB6 or WENSS match.

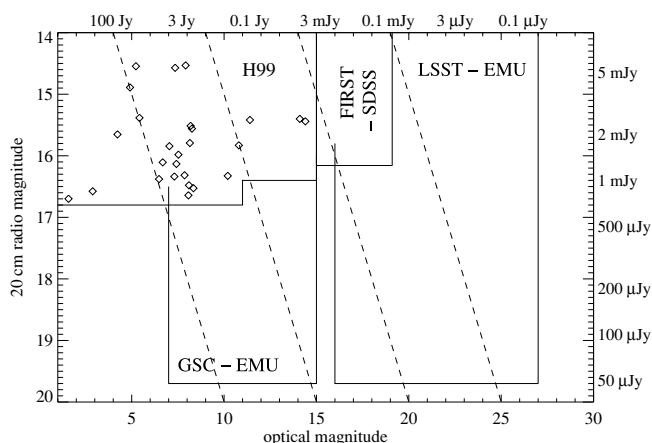


Figure 8. Parameter space probed by combinations of radio and optical surveys. Stellar radio sources detected by H99 are indicated by symbols. Dashed lines show constant radio-to-optical flux ratios of 1:1000, 1:100, 1:1, 100:1 (from left to right). The FIRST–SDSS matching corresponds to the current paper. LSST and EMU are future southern sky surveys.

stars with WD+dM bridge colors among the candidate sample. Three of the radio star candidates with WD+dM bridge colors are significantly offset from the stellar locus in the four-dimensional color space ($4DCD > 2$). Two of these three stars are magnetically active; a third star on the WD+dM bridge is also active. These four stars are good candidates for continuing investigation.

We searched for radio detections at two other wavelengths, 6 cm and 92 cm. Eight sources were detected at more than one radio wavelength. The spectral index distribution for the stellar sources is similar to the distribution for a sample of possible AGN contaminants. Therefore, the subset of stellar radio candidates may be plagued by the same AGN contamination seen in the overall sample.

This study shows that FIRST and SDSS are not a good pair of surveys for the study (or discovery) of radio stars: stars bright enough at 20 cm to appear in FIRST are probably above the $m = 15$ saturation limit of the SDSS. Figure 8 shows the radio–optical parameter space probed by the H99 study and the FIRST–SDSS correlation presented in this paper. FIRST is currently the largest deep radio survey available; the figure indicates that much fainter radio data are required in order to discover more stars of the population found by H99. A much deeper sky survey at the same frequency as FIRST is likely to be carried out in the southern hemisphere using the Australian Square Kilometer Array Pathfinder¹⁶ (ASKAP; Johnston et al. 2009). One of ASKAP’s invited proposals involves a project known as “EMU: Evolutionary Map of the Universe”¹⁷, which includes a large southern sky survey down to $50 \mu\text{Jy}$ ($5\sigma_{\text{rms}}$) at 20 cm. Although the main science driver for the ASKAP EMU project is the study of AGN and galaxy evolution, the field of radio stars will benefit immensely by cross-correlating the EMU survey with an all-sky optical survey such as the Guide Star Catalog (GSC; Lasker et al. 1990) or a large southern sky survey such as the Large Synoptic Survey Telescope¹⁸ (LSST; Ivezić et al. 2008b).

The GSC, the faintest of the optical surveys used in the H99 study, covered the sky in the approximate magnitude range of

7–15. As shown in Figure 8, the combination of the GSC and EMU will be sensitive to stars with radio-to-optical flux ratios from less than 1:1000 to those with the highest flux ratios found by H99. Covering half the sky and extending 20 times fainter in the radio than FIRST, GSC–EMU should result in the largest sample of candidate radio stars to date.

The LSST is a multi-epoch optical survey that will observe a quarter of the sky every three nights and detect point sources down to $r \sim 27$ ($r \sim 24.5$ for a single exposure). The radio–optical parameter space covered by a potential LSST–EMU matching is also shown in Figure 8. The H99 survey found only a couple of radio stars of the type to which LSST–EMU will be sensitive. The EMU survey, 20 times fainter than FIRST, will probe a 20–90 times larger volume in the Milky Way disk, and thus may find on the order of 100 new sources of faint stellar radio emission. In addition, the LSST will be able to recognize active M dwarfs via their UV flaring. This method could be more efficient than looking for $H\alpha$ emission in SDSS spectra, which are available for only about 0.25% of M dwarfs detected by the SDSS. The advent of the EMU survey to radio astronomy, combined with large optical surveys, is likely to increase the number of known radio stars by orders of magnitude.

This material is based upon work supported under a National Science Foundation Graduate Research Fellowship, and by NSF grant AST-0507259 to the University of Washington. M.S.G. thanks the Advisory Council of the Department of Astrophysical Sciences, Princeton University, for generous support through a summer student fellowship. The authors would like to thank D. Helfand and N. Thyagarajan for providing information about FIRST variability, and would also like to thank R. Osten, N. Silvestri, S. Hawley, R. Norris, and J. Bellovary for helpful discussions. We also thank an anonymous referee for suggestions that led to improvements in the content of the paper.

Funding for the SDSS and SDSS-II has been provided by the Alfred P. Sloan Foundation, the Participating Institutions, the National Science Foundation, the U.S. Department of Energy, the National Aeronautics and Space Administration, the Japanese Monbukagakusho, the Max Planck Society, and the Higher Education Funding Council for England. The SDSS Web site is <http://www.sdss.org/>.

The SDSS is managed by the Astrophysical Research Consortium for the Participating Institutions. The Participating Institutions are the American Museum of Natural History, Astrophysical Institute Potsdam, University of Basel, University of Cambridge, Case Western Reserve University, University of Chicago, Drexel University, Fermilab, the Institute for Advanced Study, the Japan Participation Group, Johns Hopkins University, the Joint Institute for Nuclear Astrophysics, the Kavli Institute for Particle Astrophysics and Cosmology, the Korean Scientist Group, the Chinese Academy of Sciences (LAMOST), Los Alamos National Laboratory, the Max-Planck-Institute for Astronomy (MPIA), the Max-Planck-Institute for Astrophysics (MPA), New Mexico State University, Ohio State University, University of Pittsburgh, University of Portsmouth, Princeton University, the United States Naval Observatory, and the University of Washington.

REFERENCES

¹⁶ <http://www.atnf.csiro.au/projects/askap/>
¹⁷ <http://www.atnf.csiro.au/people/rnorris/emu/>
¹⁸ <http://www.lsst.org>

Adelman-McCarthy, J. K., et al. 2008, *ApJS*, 175, 297
 Altenhoff, W. J., Thum, C., & Wendker, H. J. 1994, *A&A*, 281, 161

- Barvainis, R., Lehár, J., Birkinshaw, M., Falcke, H., & Blundell, K. M. 2005, *ApJ*, **618**, 108
- Bastian, T. S., & Bookbinder, J. A. 1987, *Nature*, **326**, 678
- Becker, R. H., White, R. L., & Helfand, D. J. 1995, *ApJ*, **450**, 559
- Berger, E. 2002, *ApJ*, **572**, 503
- Berger, E. 2006, *ApJ*, **648**, 629
- Berger, E., et al. 2008, *ApJ*, **676**, 1307
- Bieging, J. H., Abbott, D. C., & Churchwell, E. B. 1989, *ApJ*, **340**, 518
- Blanton, M. R., Lin, H., Lupton, R. H., Maley, F. M., Young, N., Zehavi, I., & Loveday, J. 2003, *AJ*, **125**, 2276
- Bochanski, J. J., Hawley, S. L., Reid, I. N., Covey, K. R., West, A. A., Golimowski, D. A., & Ivezić, Ž. 2009, in AIP Conf. Proc. 1094, Cool Stars, Stellar Systems and the Sun, ed. E. Stempels (Melville, NY: AIP), 977
- Bochanski, J. J., West, A. A., Hawley, S. L., & Covey, K. R. 2007, *AJ*, **133**, 531
- Chapman, J. M., Leitherer, C., Koribalski, B., Bouter, R., & Storey, M. 1999, *ApJ*, **518**, 890
- Covey, K. R., et al. 2008, *AJ*, **136**, 1778
- Covey, K. R., et al. 2007, *AJ*, **134**, 2398
- Drake, S. A. 1990, *AJ*, **100**, 572
- Drake, S. A., Abbott, D. C., Bastian, T. S., Bieging, J. H., Churchwell, E., Dulk, G., & Linsky, J. L. 1987a, *ApJ*, **322**, 902
- Drake, S. A., & Linsky, J. L. 1986, *AJ*, **91**, 602
- Drake, S. A., Linsky, J. L., & Elitzur, M. 1987b, *AJ*, **94**, 1280
- Dulk, G. A. 1985, *ARA&A*, **23**, 169
- Finlator, K., et al. 2000, *AJ*, **120**, 2615
- Fukugita, M., Ichikawa, T., Gunn, J. E., Doi, M., Shimasaku, K., & Schneider, D. P. 1996, *AJ*, **111**, 1748
- Gizis, J. E., Reid, I. N., & Hawley, S. L. 2002, *AJ*, **123**, 3356
- Gregory, P. C., Scott, W. K., Douglas, K., & Condon, J. J. 1996, *ApJS*, **103**, 427
- Güdel, M. 2002, *ARA&A*, **40**, 217
- Güdel, M., & Benz, A. O. 1996, in ASP Conf. Ser. 93, Radio Emission from the Stars and the Sun, ed. A. R. Taylor & J. M. Paredes (San Francisco, CA: ASP), 303
- Güdel, M., Benz, A. O., Catala, C., & Praderie, F. 1989, *A&A*, **217**, L9
- Güdel, M., Schmitt, J. H. M. M., & Benz, A. O. 1995, *A&A*, **302**, 775
- Gunn, J. E., et al. 1998, *AJ*, **116**, 3040
- Helfand, D. J., Schnee, S., Becker, R. H., White, R. L., & McMahon, R. G. 1999, *AJ*, **117**, 1568
- Hjellming, R. M., & Gibson, D. M. 1986, *J. Br. Astron. Assoc.*, **96**, 186
- Hoeg, E., et al. 1997, *A&A*, **323**, L57
- Hogg, D. W., Finkbeiner, D. P., Schlegel, D. J., & Gunn, J. E. 2001, *AJ*, **122**, 2129
- Ivezić, Ž., et al. 2004, *Astron. Nachr.*, **325**, 583
- Ivezić, Ž., et al. 2008a, *ApJ*, **684**, 287
- Ivezić, Ž., et al. 2008b, *SerAJ*, **176**, 1
- Johnston, S., Feain, I. J., & Gupta, N. 2009, arXiv:0903.4011
- Jurić, M., et al. 2008, *ApJ*, **673**, 864
- Kimball, A. E., & Ivezić, Ž. 2008, *AJ*, **136**, 684
- Knapp, G. R., Bowers, P. F., Young, K., & Phillips, T. G. 1995, *ApJ*, **455**, 293
- Large, M. I., Beasley, A. J., Stewart, R. T., & Vaughan, A. E. 1989, *PASA*, **8**, 123
- Lasker, B. M., Sturch, C. R., McLean, B. J., Russell, J. L., Jenkner, H., & Shara, M. M. 1990, *AJ*, **99**, 2019
- Leone, F., Umama, G., & Trigilio, C. 1996, *A&A*, **310**, 271
- Lim, J., & White, S. M. 1995, *ApJ*, **453**, 207
- Lupton, R. H., Ivezić, Z., Gunn, J. E., Knapp, G., Strauss, M. A., & Yasuda, N. 2002, *Proc. SPIE*, **4836**, 350
- Munn, J. A., et al. 2004, *AJ*, **127**, 3034
- Newell, R. T., & Hjellming, R. M. 1982, *ApJ*, **263**, L85
- Newman, P. R., et al. 2004, *Proc. SPIE*, **5492**, 533
- Osten, R. A., Hawley, S. L., Allred, J., Johns-Krull, C. M., Brown, A., & Harper, G. M. 2006, *ApJ*, **647**, 1349
- Perryman, M. A. C., et al. 1997, *A&A*, **323**, L49
- Phillips, R. B., & Titus, M. A. 1990, *ApJ*, **359**, L15
- Pier, J. R., Munn, J. A., Hindsley, R. B., Hennessy, G. S., Kent, S. M., Lupton, R. H., & Ivezić, Ž. 2003, *AJ*, **125**, 1559
- Plotkin, R. M., Anderson, S. F., Hall, P. B., Margon, B., Voges, W., Schneider, D. P., Stinson, G., & York, D. G. 2008, *AJ*, **135**, 2453
- Reid, M. J., & Menten, K. M. 1997, *ApJ*, **476**, 327
- Rengelink, R. B., Tang, Y., de Bruyn, A. G., Miley, G. K., Bremer, M. N., Roettgering, H. J. A., & Bremer, M. A. R. 1997, *A&AS*, **124**, 259
- Richards, G. T., et al. 2001, *AJ*, **121**, 2308
- Rys, S., & Machalski, J. 1990, *A&A*, **236**, 15
- Schlegel, D. J., Finkbeiner, D. P., & Davis, M. 1998, *ApJ*, **500**, 525
- Schneider, D. P., et al. 2007, *AJ*, **134**, 102
- Scranton, R., et al. 2002, *ApJ*, **579**, 48
- Silvestri, N. M., Hawley, S. L., & Oswalt, T. D. 2005, *AJ*, **129**, 2428
- Silvestri, N. M., et al. 2006, *AJ*, **131**, 1674
- Skinner, S. L., Brown, A., & Stewart, R. T. 1993, *ApJS*, **87**, 217
- Skrutskie, M. F., et al. 2006, *AJ*, **131**, 1163
- Smith, J. A., et al. 2002, *AJ*, **123**, 2121
- Smolčić, V., et al. 2004, *ApJ*, **615**, L141
- Stoughton, C., et al. 2002, *AJ*, **123**, 485
- Tucker, D. L., et al. 2006, *Astron. Nachr.*, **327**, 821
- Wendker, H. J. 1987, *A&AS*, **69**, 87
- Wendker, H. J. 1995, *A&AS*, **109**, 177
- West, A. A., Hawley, S. L., Bochanski, J. J., Covey, K. R., Reid, I. N., Dhital, S., Hilton, E. J., & Masuda, M. 2008, *AJ*, **135**, 785
- West, A. A., et al. 2004, *AJ*, **128**, 426
- White, S. M., Jackson, P. D., & Kundu, M. R. 1989, *ApJS*, **71**, 895
- White, S. M., Pallavicini, R., & Kundu, M. R. 1992, *A&A*, **257**, 557
- York, D. G., et al. 2000, *AJ*, **120**, 1579